



ISTITUTO NAZIONALE DI RICERCA METROLOGICA Repository Istituzionale

A novel magnetizer for 2D broadband characterization of steel sheets and soft magnetic composites

This is the author's accepted version of the contribution published as:

Original

A novel magnetizer for 2D broadband characterization of steel sheets and soft magnetic composites / O., d.l.B., Appino, C., F., F., M., L., C., R., P., V.. - In: INTERNATIONAL JOURNAL OF APPLIED ELECTROMAGNETICS AND MECHANICS. - ISSN 1383-5416. - 48:2-3(2015), pp. 239-245. [10.3233/JAE-151994]

Availability:

This version is available at: 11696/32656 since: 2021-02-07T07:43:58Z

Publisher:

IOS PRESS

Published

DOI:10.3233/JAE-151994

Terms of use:

This article is made available under terms and conditions as specified in the corresponding bibliographic description in the repository

Publisher copyright

(Article begins on next page)

A novel magnetizer for 2D broadband characterization of steel sheets and soft magnetic composites

O. de la Barrière^{1a}, Carlo Appino², Fausto Fiorillo², Michel Lécrivain¹, Carlo Ragusa³, Patrice Vallade¹

¹SATIE, ENS Cachan, CNRS, UniverSud, 61 av du President Wilson, F-94230 Cachan, France

²Istituto Nazionale di Ricerca Metrologica (INRIM), Strada delle cacce 91, 10135 Torino, Italy

³Dipartimento di Ingegneria Elettrica, Politecnico di Torino, C.so Duca degli Abruzzi 24, 10129 Torino, Italy

^a Corresponding author. Electronic address: barriere@satie.ens-cachan.fr, telephone: 0033147402125.

Abstract

The magnetic materials used in embedded applications need characterization and modeling in the kilohertz range. This problem is well addressed under conventional alternating induction, but with rotational and two-dimensional induction loci, which are ubiquitous in electrical machines, there is lack of results, because of the difficult task of reaching such high frequencies at technically interesting induction values with the conventional laboratory test benches. To overcome this difficulty, a novel three phase magnetizer has been designed, exploiting 3D finite element calculations, and applied in the lab. This device permits one to measure magnetization curve and losses in soft magnetic steel sheets and soft magnetic composites under alternating and circular induction up to about 5 kHz. We provide a few significant examples of loss measurements in 0.20 mm thick Fe-Si and Fe₅₀Co₅₀ laminations, and in soft magnetic composites. These measurements bring to light the role of skin effect under one- and two-dimensional fields.

13 I. INTRODUCTION

14 High speed electrical machines are very promising in terms of torque density [1] and are therefore interesting
15 for embedded applications. But, in order to achieve a correct prediction of the machine efficiency at the design
16 stage, an accurate experimental characterization of the magnetic material in the broad frequency range encountered
17 in such machines, extending up to the kHz range, is needed.

18 Reaching high frequencies at technically significant induction levels on magnetic characterization benches is
19 far from simple. The necessity of handling large powers with the magnetizing system is a demanding task,
20 especially with two-dimensional (2D) fields. In such a case, no measurement standard is available, in contrast with
21 the conventional characterization under alternating field, where one can rely, for example, on ASTM and IEC
22 standards valid up to 10 kHz [2][3]. On the other hand, two-dimensional induction loci are ubiquitous in electrical
23 machines [4] and the 2D magnetic characterization of soft magnetic materials has industrial relevance.

24 2D measurements are generally performed using either vertical-horizontal double-yoke magnetizers and square
25 samples[5][6], or a three phase magnetizer with circular/hexagonal samples [7] [8]. While lack of homogeneity of
26 the magnetic induction in the sample can be a problem [9], in all cases the test frequency at technical inductions
27 can barely attain a few hundred Hz, far from actual frequencies encountered in high speed electrical machines.

28 We discuss in this paper design and operation of a novel 2D broadband three-phase magnetizer, by which
29 superior performances up to the kHz range can be obtained. It is built around a laminated yoke, especially designed
30 through 3D finite element (FEM) calculations. By this device, magnetization curve and losses in magnetic
31 laminations and soft magnetic composite (SMC) materials under alternating and circular induction up to about 5
32 kHz can be measured. A few significant examples of loss measurements in 0.20 mm thick Fe-Si and Fe₅₀Co₅₀
33 sheets, and in SMC samples are provided and discussed.

34

35 II. DESIGN OF THE 2D MAGNETIZER

36 *A) Design constraints*

37 The minimum requirement formulated at start is that the three-phase magnetizer makes possible full
38 characterization of conventional 0.20 mm thick non-oriented Fe-Si laminations under controlled 2D flux loci up

39 to peak polarization $J_p = 1.5$ T at the frequency $f = 1$ kHz. Instrumental to the achievement of this objective is the
40 use of DC-20 kHz CROWN 5000VZ power amplifiers, by which each magnetizing phase can be supplied up to
41 maximum voltage and current peak values $V_{p,MAX} = 150$ V and $I_{p,MAX} = 40$ A.

42

43 *B) Optimizing the magnetizer geometry.*

44 A schematic view of the realized three-phase magnetizer is shown in Fig. 1. For its development, the following
45 design parameters have been imposed: 1) Circular sample of diameter $D = 80$ mm, expected to exhibit good
46 uniform induction profile, especially in the central region, where the induction and the effective magnetic field are
47 measured [10]. 2) A small airgap, to minimize both the magnetizing current in each phase and the demagnetizing
48 field. An optimal solution, taking into account the mechanical tolerances, is obtained by adopting the airgap width
49 $a = 1$ mm. 3) Homogeneous rotating field with simplest winding configuration. To this end, the three-phase two-
50 pole stator core was designed with three slots per pole and per phase (totalling 18 slots). To avoid winding
51 overhang crossing, a toroidal winding configuration [11] was adopted (see Fig. 1). 4) Laminated stator core, built
52 out of 0.35 mm thick stacked non-oriented Fe-Si sheets. The details of the windings are given in Fig. 2, where
53 each coil occupies a slot and is series connected with all the other coils of the same phase. If n_s is the number of
54 turns per coil (i.e. the number of conductors per slot), each phase is made of $6 \cdot n_s$ turns in series. To achieve the
55 desired magnetizer performances, the following geometrical parameters, shown in Fig. 1, were optimized: the slot
56 depth t_s , the slot width w_s , the back-core thickness t_Y , and the active axial height T of the core. A convenient
57 number n_s of copper turns per slot was assumed. With maximum magnetizing current density of 5 A/mm², as
58 required to avoid overheating, the values $t_s = 20$ mm and $w_s = 5$ mm are chosen. At the same time, t_Y is set to
59 25 mm, making the maximum flux density in the back-core around 0.2 T and the associated energy losses
60 negligible. To calculate the dependence of value and homogeneity of the generated rotating magnetic field and
61 sample induction on the ratio between yoke height and sample thickness T/d , a 3D non-linear magnetostatic FEM
62 modelling is implemented, where the magnetic constitutive equations of yoke sheets and test sample are identified
63 with the corresponding experimental anhysteretic curves. When carrying out such numerical simulation, the
64 number of turns per slot n_s is not already known, and therefore each coil is modelled by a single copper turn with

65 the magnetomotive force nsI_p . This calculated magnetomotive force per slot nsI_p providing a defined rotating peak
66 induction $B_p = 1.5$ T in the 0.20mm thick Fe-Si sample sheet at $f = 1$ kHz is shown in Fig. 3 as a function of T/d .
67 The same figure shows the corresponding trend of the peak flux, normalized to the number of turns per slot Φ_p/ns .
68 Φ_p is the sum of the contributions by the six series-connected coils. As expected, the required magnetomotive force
69 nsI_p decreases with increasing the ratio T/d , to reach a more or less asymptotic value beyond $T/d \cong 80$. Here the
70 effect of flux fringing becomes negligible and the quantity Φ_p/ns tends to rapidly increase with T/d , following the
71 corresponding increase of the cross-sectional area of the core. Given these trends of nsI_p and Φ_p/ns , their product
72 $\Phi_p I_p$, that is the apparent power $\pi/\Phi_p I_p$, passes through a minimum. This occurs for $T/d \cong 75$ (corresponding to $T =$
73 15 mm), where the normalized flux $\Phi_p/ns \cong 2$ mWb and $nsI_p \cong 100$ A. Consequently, one obtains that the normalized
74 peak voltage at 1 kHz is $V_p/ns = 2\pi/\Phi_p/ns \cong 12.6$ V. With $I_p = 10$ A and $ns = 10$, the voltage drop $V_p = 127$ V is
75 safely within the power supply capabilities. Higher frequencies can actually be reached by changing $ns = 10$ to ns
76 $= 5$ via a mid-point connection predisposed on each coil. The accordingly built three-phase magnetizer, which is
77 endowed with an air-cooling system, is shown in Fig. 4. It has been tested using a calibrated hysteresisgraph-
78 wattmeter, where a defined 2D induction loci can be imposed by digital feedback [12]. Fig. 5 compares recorded
79 and FEM calculated current and voltage waveforms in one phase of the magnetizer at $f = 1$ kHz under imposed
80 circular induction of amplitude $B_p = 1.0$ T. This is detected upon a 20 mm wide central region of the 80mm diameter
81 0.20 mm thick Fe-Si sample. It is observed that the current waveform is accurately predicted by the FEM
82 calculations, whereas the voltage drop is slightly underestimated. This is due to the fact that the actual windings
83 have somewhat higher overhang than the idealized windings considered in the FEM analysis (see Fig. 1), because
84 of the mechanical rigidity of the copper wire. This implies higher inductance, that is higher voltage drop, than
85 predicted by the numerical model, but no practical consequences on the stated objectives of the design are
86 observed.

87 III. RESULTS: A FEW EXAMPLES

88 Test measurements have been performed on Fe-Si and Fe-Co sheets and on soft magnetic composites with the
89 fieldmetric method [7]. For measurements beyond a few hundred Hz, the employed H -coil is wound with well

90 separated turns, minimizing the stray capacitances. The 3D FEM analysis shows that upon the central 20 mm
91 measuring square region of the disk samples the homogeneity of the effective field is better than 2 %.

92 The non-oriented Fe-Si and Fe-Co 0.20 mm thick sheets have been characterized under alternating and rotating
93 field up to $J_p = 1.55$ T at $f = 2$ kHz and $J_p = 2.1$ T at $f = 5$ kHz, respectively. An example of measured alternating
94 $W^{(ALT)}$ and rotational $W^{(ROT)}$ energy loss behaviour versus frequency and peak polarization J_p in the Fe-Co sheets
95 is shown in Fig. 6a. It is noted how the maximum of the rotational loss occurs at increasing J_p values with
96 increasing the magnetizing frequency. This occurs because of the increasing proportion of the classical loss
97 component W_{class} , which, contrary to the other components, the domain wall related hysteresis W_{hyst} and excess W_{exc}
98 losses, monotonically increases with J_p [7]. However, loss separation is not easily treated under broadband
99 conditions, because skin effect may arise and the standard equation of the classical energy loss, which is written
100 as $W_{class}(J_p, f) = k \frac{\pi^2}{6} \cdot \sigma d^2 B_p^2 f$, where σ is the conductivity ($k = 1$ for alternating sinusoidal induction, $k = 2$
101 for circular induction) will not apply beyond a certain upper frequency f_{lim} . It is indeed interesting to see how one
102 can easily find f_{lim} by loss separation. It is a unique simple way to detect the surge of the skin effect. According to
103 the statistical theory of losses and the previous equation for W_{class} , it is predicted that $W_{diff} = W_{hyst} + W_{exc}$ is
104 proportional to $f^{1/2}$ [13]. Fig. 6b, showing the behaviour of W_{diff} at $J_p = 1$ T versus $f^{1/2}$ up to $f = 5$ kHz, shows that
105 such a prediction is satisfied up to $f = f_{lim} \cong 400$ Hz. Beyond this frequency, W_{class} is overestimated by the previous
106 equation and the calculated W_{diff} strongly deviates from the $f^{1/2}$ behavior.

107 Further experiments have been performed on SMC samples. These materials are made of bonded and pressed
108 iron particles, typically 10 μ m to 100 μ m wide. Because of their isotropic properties, they can handle 3D fluxes,
109 besides being attractive for high frequency applications. Fig. 7 shows an example of energy loss versus frequency
110 measured under alternating (sinusoidal) and circular polarization up to 4 kHz, in 80 mm diameter 3 mm thick disk
111 samples. The non-linear increase of $W^{(ALT)}$ and $W^{(ROT)}$ with f can be observed also in these materials. The relatively
112 large sample thickness, required for mechanical reasons, combines with intrinsically low permeability values to
113 impose, for a same apparent power of the magnetizing system, pretty lower $J_p \cdot f_{max}$ products than in sheet samples.
114 Examples of such limits are $J_p \cdot f_{max} = 1.25$ T·1 kHz or $J_p \cdot f_{max} = 1.0$ T·2 kHz. They are nonetheless quite larger

115 than those obtained in the recent literature (e.g. $J_p \cdot f_{\max} = 0.77 \text{ T} \cdot 1 \text{ kHz}$) [14].

116 **IV. CONCLUSIONS**

117 A new magnetizer, associated with digitally controlled hysteresisgraph/wattmeter, has been developed for the
118 broadband alternating and two-dimensional characterization of soft magnetic sheets and composites deep into the
119 kHz range. This device, largely overcoming the upper polarization and frequency limits reported so far in the
120 literature for similar apparatus, has been designed and optimized by 3D FEM calculations. With the high frequency
121 range made available to the 2D measurements, the skin effect in magnetic laminations under rotating induction
122 has been unambiguously put in evidence for the first time. The non-linear increase of the energy loss with the
123 magnetizing frequency is also demonstrated in the soft magnetic composites.

124

- 126 [1] S. Niu, S. Ho, W. Fu, and J. Zhu, *IEEE Trans. Magn.*, **48** (2012) 1007-1010.
127 [2] IEC Standard Publication 60404-10, Methods of measurement of magnetic properties of magnetic steel sheet
128 and strip at medium frequencies, 1988, Geneva, IEC Central Office.
129 [3] ASTM Publication A348/A348M, Standard test method for alternating current magnetic properties of
130 materials using the wattmeter-ammeter-voltmeter method, 100 to 10 000 Hz and 25-cm Epstein frame, 2011,
131 West Conshohocken, PA.
132 [4] O. Bottauscio, M. Chiampi, A. Manzin, and M. Zucca, *IEEE Trans. Magn.*, **40** (2004) 3254-3261.
133 [5] J.G. Zhu and V.S. Ramsden, *IEEE Trans. Magn.*, **29** (1993) 2995-2997.
134 [6] A.J. Moses, *IEEE Trans. Magn.*, **30** (1994) 902-906.
135 [7] C. Appino, F. Fiorillo, and C. Ragusa, *J. Appl. Phys.*, **105** (2009) 07E718.
136 [8] A. Hasenzagl, B. Weiser, and H. Pfützner, *J. Magn. Magn. Mater.*, **160** (1996) 180-182.
137 [9] N. Nencib, A. Kedous-Lebouc, and B. Cornut, *IEEE Trans. Magn.*, **31** (1995) 3388-3390.
138 [10] Y. Guo, J. G. Zhu, J. Zhong, H. Lu, and J. X. Jin, *IEEE Trans. Magn.*, **44** (2008) 279-291.
139 [11] R. Qu, M. Aydin, and T.A. Lipo, "Performance comparison of dual-rotor radial-flux and axial-flux
140 permanent-magnet BLDC machines," in *IEEE Electric Machines and Drives Conference (IEMDC)*, 2003.
141 [12] C. Ragusa and F. Fiorillo, *J. Magn. Magn. Mater.*, **304** (2006), e568-e570.
142 [13] G. Bertotti, *IEEE Trans. Magn.*, **24** (1988) 621-630.
143 [14] Y. Guo, J. Zhu, H. Lu, Z. Lin, and Y. Li, *IEEE Trans. Magn.*, **48** (2012) 3112-3115.
144

Figures captions

Fig. 1. 3D finite element model of the three-phase magnetizer and its main geometrical parameters.

Fig. 2. Details of the three phase magnetizer windings.

Fig. 3. Magnetomotive force per slot nsI_p and resulting peak flux per turn Φ_p/ns as a function of core to sample thickness ratio T/d for a rotating peak induction $B_p = 1.5$ T at $f = 1$ kHz in a 0.20 mm thick non-oriented Fe-Si sheet sample. Minimum supply power $\pi f \Phi_p I_p$ is required for $T/d \cong 75$.

Fig. 4. The realized 2D three-phase magnetizer.

Fig. 5. Measured and FEM calculated current $i(t)$ circulating in a phase of the stator and corresponding voltage $v(t)$ waveforms for rotating induction $B_p = 1$ T at 1 kHz in a 0.20 mm thick non-oriented Fe-Si sheet sample.

Fig. 6. Examples of alternating ($W^{(ALT)}$) and rotational ($W^{(ROT)}$) energy loss measurements performed with the novel 2D broadband magnetizer. (a) $W^{(ALT)}$ and $W^{(ROT)}$ measured at three different frequencies in a 0.20 mm thick Fe-Co sheet sample versus peak polarization. (b) The quantity $W_{diff} = W - W_{class}$, where W_{class} is the classical loss calculated according to the standard formula for uniform induction in the sample cross-section, shows strong deviation from the expected linear dependence on $f^{1/2}$ beyond about 400 Hz, signaling the surge of the skin-effect.

Fig. 7. Alternating and rotational energy loss versus frequency at different polarization values in a commercial soft magnetic composite. The measurements are performed on 80 mm diameter 3 mm thick disk samples.

Figures

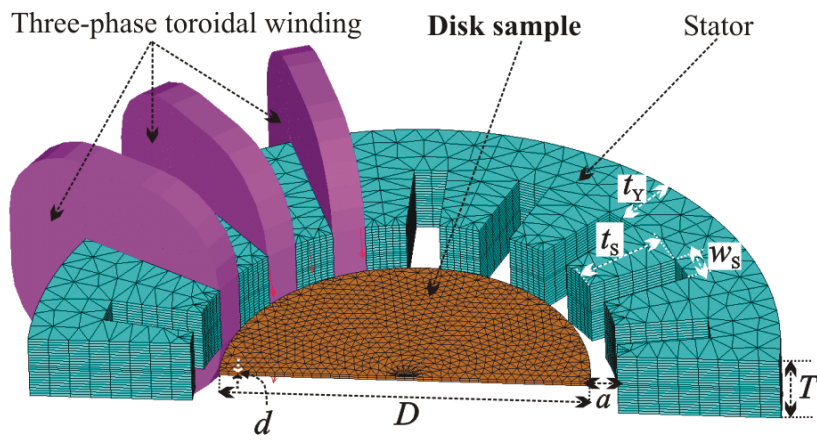
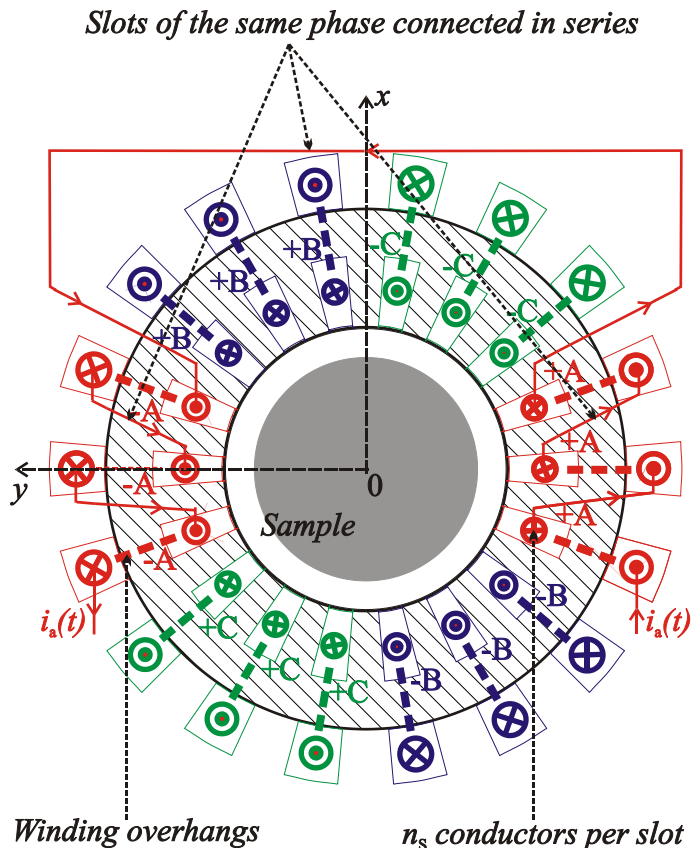


Fig. 1



172
173

Fig. 2

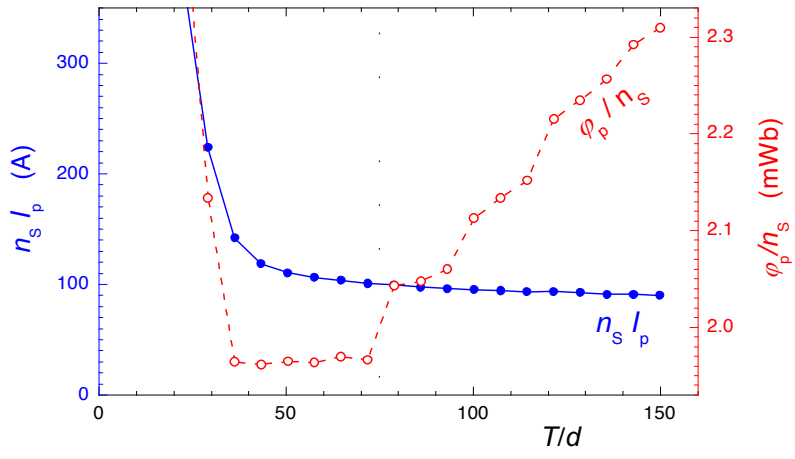


Fig. 3

174
175

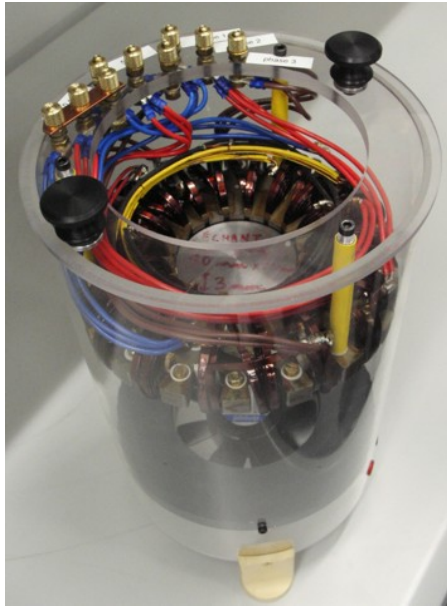
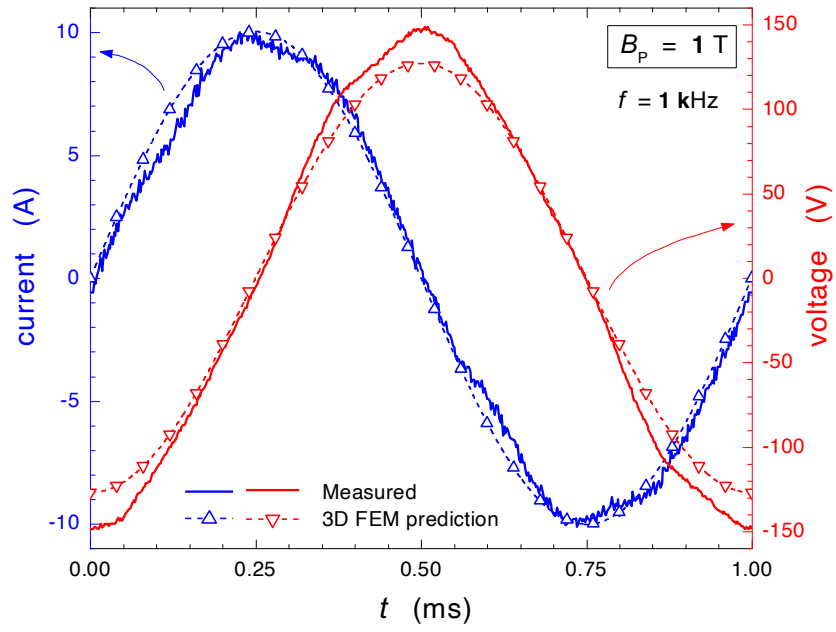


Fig. 4

176
177



178

179

Fig. 5

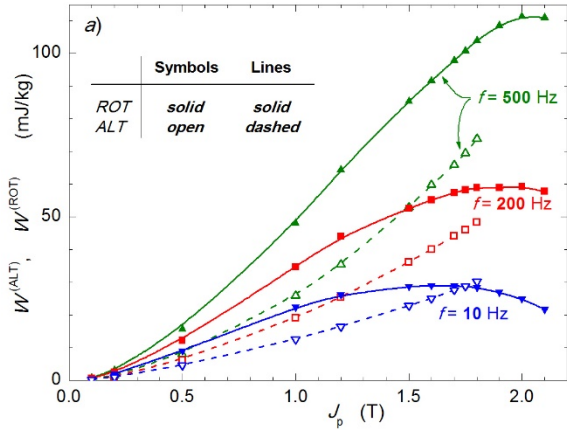
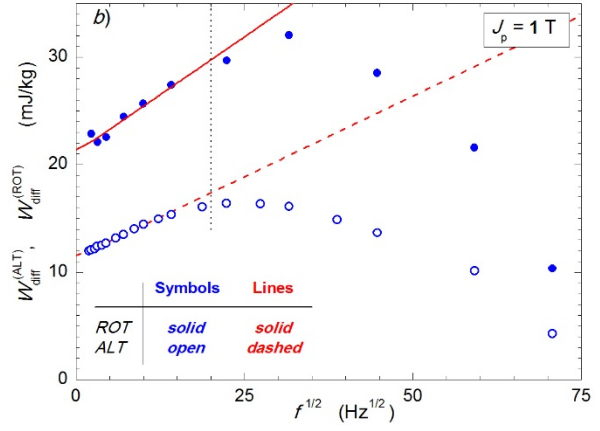


Fig. 6



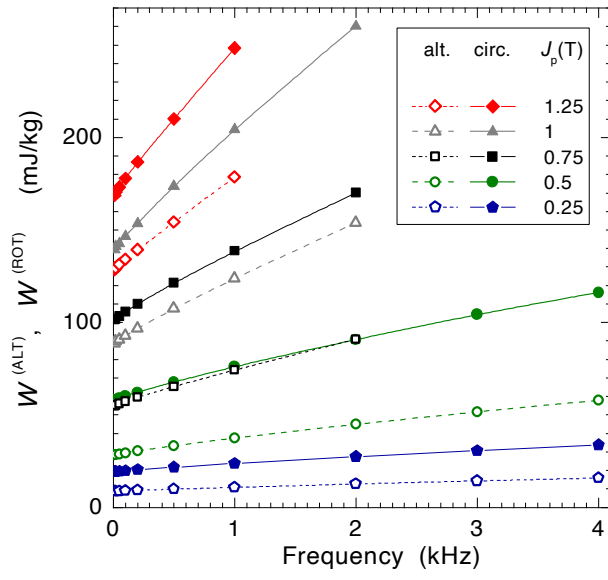


Fig. 7

181

182

183